Compressive Sensing-based Harmonic Sources Identification in Smart Grids

Daniele Carta, *Student Member, IEEE*, Carlo Muscas, *Senior Member, IEEE*, Paolo Attilio Pegoraro, *Senior Member, IEEE*, Antonio Vincenzo Solinas, Sara Sulis, *Senior Member, IEEE*

***Abstract*— Identifying the prevailing polluting sources would help the distribution system operators in acting directly on the cause of the problem, thus reducing the corresponding negative effects. Due to the limited availability of specific measurement devices, ad-hoc methodologies must be considered. In this regard, Compressive Sensing-based solutions are perfect candidates. This mathematical technique allows recovering sparse signals when a limited number of measurements are available, and thus overcoming the lack of Power Quality meters.**

In this paper, a new formulation of the ℓ_1-minimization algorithm for Compressive Sensing problems, with quadratic constraint, has been designed and investigated in the framework of the identification of the main polluting sources in Smart Grids. A novel whitening transformation is proposed for this context. This specific transformation allows the energy of the measurement errors to be appropriately estimated and thus better identification results are obtained. The validity of the proposal is proved by means of several simulations and tests performed on two distribution networks for which suitable measurement systems are considered along with a realistic quantification of the uncertainty sources.

***Index Terms*—Compressed sensing; Harmonic analysis, Harmonic distortion; Harmonic Source Estimation; Matching pursuit algorithms; Power distribution; Power Quality; Smart Grids.**

I. Introduction

The evolution of distribution grids into new generation networks, known as Smart Grids (SGs), is leading to numerous changes in the behaviour of these systems. In particular, the increasing presence of non-linear loads and distributed generators, mostly power electronics-based, contributes to the increment of the harmonic pollution in the network. Consequently, different problems arise, such as unexpected failures of sensitive devices, increase of power losses, increase of the management costs and so on [1].

Different solutions to monitor the state of the network in terms of harmonics have been proposed in literature [2]–[5], but their implementation in real networks is not always possible. These techniques require the direct monitoring of the system, and, due to the large size of the distribution systems, and the costs of Power Quality (PQ) meters, it is not always feasible to deploy them, unless highly uncertain pseudo-measurements are used to integrate the available measurements. In this regard, alternative solutions for harmonic estimation in power systems have been proposed, such as machine learning-based techniques [6], [7], wavelet-based solutions [8] and many others [9].

In this paper, the final goal is the identification of the harmonic sources, which would allow system operators to act directly on the cause of the problem. This approach, called Harmonic Source Estimation (HSoE), was presented in [10], [11], specifically for distribution networks. Due to the characteristics of the problem (under-determined systems, consequent to the limited number of measurements, and sparse state vectors), in [12] and [13] the Compressive Sensing (CS) was applied in the framework of HSoE. This recent mathematical technique is applied in many fields of science with very promising results, from image reconstruction for medical applications [14], [15] to pattern recognition [16], and communication systems [17]. In particular, the algorithms in [13] can be applied to both generic analysis (considering multiple harmonic orders at the same time) and specific analysis (focused on a single harmonic order). These solutions are meant to be directly implemented in a SG scenario, and thus are based on the use of modern measurement devices, capable to provide synchronized harmonic phasor measurements, such those proposed in [18] and [19].

The accuracy of the harmonic measurements plays a key role in the source detection, as well as in any other PQ application. For example, the ratio of inductive Voltage and Current Transformers (respectively VTs and CTs) is typically defined only at rated frequency, whereas the metrological characteristics of these transducers tend to decrease in presence of non-sinusoidal signals [20]. Recent works in literature [21], [22] have underlined how the output of measurement transducers could be compensated in harmonic measurements.

Since the CS problem can be approached with different techniques, in [23] the performance of two CS-based algorithms, Block Orthogonal Matching Pursuit (BOMP) and ℓ_1-minimization, applied to the HSoE analysis have been evaluated, under different measurement uncertainty conditions. Both BOMP and ℓ_1-minimization are largely applied for recovering sparse signals, due to their specifications. The BOMP is often chosen due to the ease of implementation and the low computational burden, whereas ℓ_1 algorithms are typically slower but provide more accurate results. In fact, in

Dr. Pegoraro work was partially funded by Fondazione di Sardegna for the research project "SUM2GRIDS, Solutions by mUltidisciplinary approach for intelligent Monitoring and Management of power distribution GRIDS".

D. Carta, C. Muscas, P. A. Pegoraro, A. V. Solinas, and S. Sulis are with the Department of Electrical and Electronic Engineering of the University of Cagliari, Piazza d'Armi, 09123 Cagliari, Italy (email: [daniele.carta, carlo.muscas, paolo.pegoraro, v.solinas, sara.sulis]@unica.it).

 DOI:10.1109/TIM.2020.3036753
Publisher version:https://ieeexplore.ieee.org/document/9252160

[23] it has been shown that the BOMP algorithm is particularly sensitive to measurement errors, especially with reference to phase angle measurements, whereas the ℓ_1 algorithm proved to be more stable against the variation of the measurement uncertainties, and thus it is the most promising candidate for HSoE applications.

This paper is the technical extension of the paper [23], and aims at further improving the performance of the ℓ_1-minimization approach considered in [23] (here referred to as $(P1)$), exploiting the proper modelling of the measurement uncertainties. With reference to the general formulations of the ℓ_1-minimization problems, in [24] the effect of noise has been considered through the so-called $(P2)$ formulation, whose solution relies on the definition of an error energy bound.

Based on these results, in this paper, a new ℓ_1-minimization algorithm for HSoE is presented. The proposed method is based on a novel formulation of HSoE problem, referred to as $(P2)$ in the following, which is tailored for the specific context. In fact, it includes appropriate information on the boundaries of the synchronized harmonic measurement errors. Furthermore, a whitening transformation able to maintain information on the measurement error distributions is proposed, thus allowing the accurate definition of a measurement error energy bound necessary to tune $(P2)$. The paper includes a discussion on the theoretical aspects concerning measurement uncertainties involved in the definition of the algorithm and their validation through appropriate tests. Among others, the whitening transformation properties are statistically validated. The proposed algorithm overcomes the limits of HSoE algorithm $(P1)$ presented in [23] thanks to the new uncertainty modeling. Its performance is verified by testing it on simulated distribution test grids, assuming the presence of suitable measurement systems and considering different accuracy scenarios.

II. Estimation Framework

A. Harmonic Source Estimation Model

The identification of the harmonic sources in a SG can be carried out by estimating the harmonic contribution injected into the network by each source, load or generator, for all the harmonic orders of interest. In fact, given the generic harmonic order h, it is possible to formulate the problem as the following linear model:

$$\overline{\mathbf{y}}_h = \overline{\mathbf{A}}_h \overline{\mathbf{u}}_h + \overline{\mathbf{e}}_h \tag{1}$$

where $\overline{\mathbf{y}}_h \in \mathbb{C}^M$ represents the vector of the M harmonic phasor measurements, voltage and/or current, with reference to the harmonic order h, whose corresponding measurement errors are represented with vector $\overline{\mathbf{e}}_h \in \mathbb{C}^M$. The measurement matrix $\overline{\mathbf{A}}_h \in \mathbb{C}^{M\times N}$ relates the measurements to the vector $\overline{\mathbf{u}}_h \in \mathbb{C}^N$ of the N unknown harmonic currents injected by each potential source. Since the measurement matrix is obtained by considering both lines and loads, its entries change when different harmonic orders are considered, due to the changes in the model of the network. As already mentioned, the so-called "forcing" vector $\overline{\mathbf{u}}_h$ is populated with the harmonic contributions of each source, whose values can vary significantly due to the different levels of pollution provided by every source. Consequently, based on the level of injected pollution, it is possible to distinguish between poorly/non-polluting sources and mainly/prevailing polluting sources. The first group is typically the largest one, and, by neglecting the contributions of these sources, it is possible to obtain an unknown sparse vector.

The model in (1) can be also expressed in terms of real and imaginary components of both vectors and matrices. This formulation, based on real vectors, is appropriate when evaluating the impact of the measurement uncertainties, as it will be presented in Section III. In particular, by denoting with the superscripts r and x, respectively, the real and the imaginary entries, the system in (1) becomes:

$$\mathbf{y}_h = \begin{bmatrix}\mathbf{y}_h^r \\ \mathbf{y}_h^x\end{bmatrix} = \begin{bmatrix}\mathbf{A}_h^r & -\mathbf{A}_h^x \\ \mathbf{A}_h^x & \mathbf{A}_h^r\end{bmatrix}\begin{bmatrix}\mathbf{u}_h^r \\ \mathbf{u}_h^x\end{bmatrix} + \begin{bmatrix}\mathbf{e}_h^r \\ \mathbf{e}_h^x\end{bmatrix} = \mathbf{A}_h\mathbf{u}_h + \mathbf{e}_h \tag{2}$$

where $\mathbf{y}_h^r \triangleq \Re[\overline{\mathbf{y}}_h] = [y_{h,1}^r, \ldots, y_{h,M}^r]^T$ denotes the real part of the measurement vector, with the superscript T representing the transpose operation, and $\mathbf{y}_h^x \triangleq \Im[\overline{\mathbf{y}}_h] = [y_{h,1}^x, \ldots, y_{h,M}^x]^T$ denotes the corresponding imaginary part. Same considerations hold for the other vectors and matrices in (2).

In the following, for sake of simplicity, the subscript h will be omitted, since all the considerations will refer to a single harmonic order.

B. Compressive Sensing Algorithms

Compressive Sensing, also called Compressed Sensing, is a mathematical technique that allows sparse signals to be sensed by requiring a limited amount of input information. A generic vector $\mathbf{u}$ is sparse if its quasi-norm $\|\mathbf{u}\|_0$, where $\|\cdot\|_\alpha$ denotes the ℓ_α norm, is lower than its cardinality. In particular, the number of S non-zero entries in $\mathbf{u}$ denotes its sparsity level: the vector is defined S-sparse, and it is: $\|\mathbf{u}\|_0 \leq S < dim(\mathbf{u})$. Furthermore, a non-sparse vector could admit a sparse representation when represented in a different base or, as in the identification of the prevailing harmonic sources, if the entries of a vector are characterized by different orders of magnitude, those with lower value can be neglected and considered as zero. These vectors are thus termed compressible, approximately sparse or relatively sparse, and CS theory can still be applied to recover the prevailing entries.

The basis formulation of CS consists in a minimization of a ℓ_0 norm (the same symbols as in the previous section are here used for the sake of simplicity):

$$(P0)\ \min \|\mathbf{u}\|_0\ s.t.\ \mathbf{A}\mathbf{u} = \mathbf{y} \tag{3}$$

This problem is NP-hard to solve with any classic combinatorial problems solver [25], but the sparse vector can be also recovered through approximated techniques.

One of the most commonly implemented algorithms for CS application is the Orthogonal Matching Pursuit (OMP) [26]. This greedy algorithm is often chosen due to its ease of implementation and the fast computation. It is in fact an iterative algorithm that performs as many iterations as the

number of non-zero entries one wants to recover. During each iteration, the OMP selects the most correlated column of the measurement matrix to the residuals, adds it to a temporary matrix and uses it to both estimate a new non-zero entry and update the ones estimated in the previous iterations.

Another common approach consists in approximating (3) with a ℓ_1-minimization problem. In literature ([27], [28]), it has been shown that, in absence of measurement errors, if the measurement matrix obeys the Restricted Isometry Property (RIP), an unknown vector $\mathbf{u}$ can be recovered by solving the following $(P1)$ problem:

$$(P1)\ \min \|\mathbf{u}\|_1\ \ s.t.\ \mathbf{A}\mathbf{u} = \mathbf{y} \tag{4}$$

It is evident that real observations are always characterized by errors, which cannot be neglected. In this regard, in [24] the $(P1)$ problem was readdressed by including information on the perturbation on the observations:

$$(P2)\ \min \|\mathbf{u}\|_1\ \ s.t.\ \|\mathbf{A}\mathbf{u} - \mathbf{y}\|_2 \leq \epsilon \tag{5}$$

where ϵ represents the bound of the norm of the error vector. In this formulation, the definition of the optimization parameter ϵ plays a key role in the recovery process. In fact, if ϵ is correctly determined, the $(P2)$ formulation performs better than $(P1)$ under noisy conditions, as proved in [24].

Since the definition of ϵ is not trivial, in the following, a theoretical approach for its evaluation in the case of HSoE is presented and then validated through simulations.

III. Error Energy Evaluation

In the previous section, two different formulations of the ℓ_1-minimization approach have been presented, respectively labelled as $(P1)$ and $(P2)$. These formulations are here applied to HSoE. In particular, while $(P1)$ addresses the ℓ_1-minimization of an exact linear under-determined system, the $(P2)$ formulation considers a more realistic approximated linear system:

$$\mathbf{A}\mathbf{u} \simeq \mathbf{y} \tag{6}$$

where the misfit between the harmonic measurement vector $\mathbf{y}$ and the model $\mathbf{A}\mathbf{u}$ is ℓ_2-bounded, with the drawback of an increase in computational complexity. More specifically, the measurement error vector in (2) and the error bound in (5) are related, thus:

$$\xi_{\mathbf{e}} = \|\mathbf{e}\|_2^2 \leq \epsilon^2 \tag{7}$$

where $\xi_{\mathbf{e}} = \|\mathbf{e}\|_2^2$ is the energy of the harmonic phasor measurement error vector in rectangular components, hereinafter referred to as "error energy". Moreover, if the mean $\mu_{\xi_{\mathbf{e}}}$ and the standard deviation $\sigma_{\xi_{\mathbf{e}}}$ of the error energy distribution are known, the corresponding bound can be chosen according to $\epsilon^2 = \mu_{\xi_{\mathbf{e}}} + \lambda\sigma_{\xi_{\mathbf{e}}}$ where λ allows changing the confidence level associated with the inequality $\|\mathbf{e}\|_2^2 \leq \mu_{\xi_{\mathbf{e}}} + \lambda\sigma_{\xi_{\mathbf{e}}}$ (typically $\lambda \geq 2$ is needed to have a high probability).

It is worth underlying that in [24] the computation of mean and standard deviation of the noise is straightforward, since it is assumed that all the entries in the error vector follow the same (and known) distribution, Gaussian or uniform, with the same mean value and standard deviation. Same hypothesis does not hold when evaluating harmonics in power systems, due to the following main reasons:

1) harmonic measurements are characterized by different behaviours, due to the differences in the measured quantities (voltages and currents) and the measured parameters (magnitude and phase angle);
2) due to the transformations performed in (2), the distributions of the entries in the final measurement vector differ from the originals, and are unknown. This holds also for the entries of the corresponding measurement error vector.

The first problem is well known, and addressed by means of the whitening transformation presented in the following.

A. Whitening transformation

In order to take into account properly the accuracy of each measurement, it is necessary to perform the so-called "whitening" transformation. This procedure allows, through the left-multiplication of (2) by a square whitening matrix $\mathbf{W}$ (also in this case subscript h will be omitted for simplicity), weighting each measurement according to its uncertainty. In fact, the entries of $\mathbf{W}$ are defined such that the transformation allows assigning lower weights to the measurements with higher uncertainties, and vice versa.

Performing a whitening transformation means applying a linear transformation to the random vector $\mathbf{y}$ in order to obtain a new random vector $\mathbf{y}_w$, having the identity matrix as covariance matrix, that is $\mathbf{\Sigma}_{\mathbf{y}_w} = \mathbf{I}$.

The covariance matrix of a column vector is defined as:

$$\mathbf{\Sigma}_{\mathbf{y}} = E[\mathbf{y}\mathbf{y}^T] \tag{8}$$

where the symbol E is the expectation operator. Thus, it is possible to observe that:

$$\begin{gathered} \forall\, \mathbf{W} : \mathbf{W}^T\mathbf{W} = \mathbf{\Sigma}_{\mathbf{y}}^{-1} \\ \mathbf{y}_w \triangleq \mathbf{W}\mathbf{y} \Longrightarrow \mathbf{\Sigma}_{\mathbf{y}_w} = \mathbf{I} \end{gathered} \tag{9}$$

Given the i-th generic measured phasor, with magnitude ρ_i and phase angle ϕ_i, its corresponding real and imaginary components, respectively y_i^r and y_i^x, can be obtained with the non-linear transformation:

$$\begin{aligned} y_i^r &= \rho_i \cos(\phi_i) \\ y_i^x &= \rho_i \sin(\phi_i) \end{aligned} \tag{10}$$

whose Jacobian matrix, around the measurement point, is $\mathbf{J}$:

$$\mathbf{J}_i = \begin{bmatrix} \cos\phi_i & -\rho_i \sin\phi_i \\ \sin\phi_i & \rho_i \cos\phi_i \end{bmatrix} \tag{11}$$

By considering the standard deviations of both magnitude and phase, respectively denoted by σ_{ρ_i} and σ_{ϕ_i}, it is possible to obtain the corresponding 2×2 covariance matrix:

$$\mathbf{\Sigma}_{\rho_i,\phi_i} = \begin{bmatrix} \sigma_{\rho_i}^2 & 0 \\ 0 & \sigma_{\phi_i}^2 \end{bmatrix} \tag{12}$$

and, through the application of the uncertainty propagation law [29], the covariance matrix referred to the corresponding real and imaginary components:

$$\boldsymbol{\Sigma}_{y_i^r,y_i^x} = \mathbf{J}_i \begin{bmatrix} \sigma_{\rho_i}^2 & 0 \\ 0 & \sigma_{\phi_i}^2 \end{bmatrix} \mathbf{J}_i^T = \\ = \begin{bmatrix} \rho_i^2\sigma_{\phi_i}^2 \sin\phi_i^2 + \sigma_{\rho_i}^2 \cos\phi_i^2 & (\sigma_{\rho_i}^2 - {\rho_i}^2\sigma_{\phi_i}^2)\sin\phi_i\cos\phi_i \\ (\sigma_{\rho_i}^2 - \rho_i^2\sigma_{\phi_i}^2)\sin\phi_i\cos\phi_i & \rho_i^2\sigma_{\phi_i}^2\cos\phi_i^2 + \sigma_{\rho_i}^2\sin\phi_i^2 \end{bmatrix} \tag{13}$$

By extension, assuming that magnitude and phase angle measurement errors for all the measured phasors are uncorrelated, it is possible to obtain the covariance matrix of the overall measurement vector $\boldsymbol{\Sigma}_{\mathbf{y}}$ as:

$$\boldsymbol{\Sigma}_{\mathbf{y}} = \mathbf{J}\boldsymbol{\Sigma}_{\boldsymbol{\rho},\boldsymbol{\phi}}\mathbf{J}^T \tag{14}$$

where $\boldsymbol{\Sigma}_{\mathbf{y}}$ is the covariance matrix of all the real and imaginary parts of the considered phasor measurements, and $\mathbf{J}$ is the Jacobian matrix of overall transformation. It is worth underlying that, if all the M measured phasors are considered uncorrelated, the overall covariance matrix in amplitude and phase, $\boldsymbol{\Sigma}_{\boldsymbol{\rho},\boldsymbol{\phi}}$, is diagonal. Thus, by defining its inverse square root as follows:

$$\boldsymbol{\Sigma}_{\boldsymbol{\rho},\boldsymbol{\phi}}^{-\frac{1}{2}} = \begin{bmatrix} \sigma_{\rho_1}^{-1} & & & & & 0 \\ & \ddots & & & & \\ & & \sigma_{\rho_M}^{-1} & & & \\ & & & \sigma_{\phi_1}^{-1} & & \\ & & & & \ddots & \\ 0 & & & & & \sigma_{\phi_M}^{-1} \end{bmatrix} \tag{15}$$

it is possible to notice that an infinite number of whitening matrices that satisfy (9) are available. In fact, given any orthogonal matrix $\mathbf{Q} \in \mathbb{R}^{2M\times 2M}$, it is possible to observe that:

$$\begin{aligned} \boldsymbol{\Sigma}_{\mathbf{y}}^{-1} =& \mathbf{J}^{-T}\boldsymbol{\Sigma}_{\boldsymbol{\rho},\boldsymbol{\phi}}^{-\frac{1}{2}}\boldsymbol{\Sigma}_{\boldsymbol{\rho},\boldsymbol{\phi}}^{-\frac{1}{2}}\mathbf{J}^{-1} = \\ =& (\mathbf{J}^{-T}\boldsymbol{\Sigma}_{\boldsymbol{\rho},\boldsymbol{\phi}}^{-\frac{1}{2}}\mathbf{Q}^T)(\mathbf{Q}\boldsymbol{\Sigma}_{\boldsymbol{\rho},\boldsymbol{\phi}}^{-\frac{1}{2}}\mathbf{J}^{-1}) \\ & \forall\mathbf{Q} : \mathbf{Q}\mathbf{Q}^T = \mathbf{Q}^T\mathbf{Q} = \mathbf{I} \end{aligned} \tag{16}$$

where the whitening matrices can be defined as:

$$\mathbf{W}_Q \triangleq \mathbf{Q}\boldsymbol{\Sigma}_{\boldsymbol{\rho},\boldsymbol{\phi}}^{-\frac{1}{2}}\mathbf{J}^{-1} \tag{17}$$

In [13] and [23], the matrix allowing the whitening of the measurements has been obtained by means of the Cholesky factorization of the overall covariance matrix, $\boldsymbol{\Sigma}_{\mathbf{y}} = \mathbf{U}_C^T\mathbf{U}_\mathbf{C}$, and assigning $\mathbf{W}_C = \mathbf{U}_C^{-T}$, which satisfies (9). Thus, by denoting with the subscript w_C the result of the whitening transformation through the Cholesky factorization, the system with the whitened measurements results in:

$$\begin{aligned} \mathbf{y}_{w_C} \triangleq \mathbf{W}_C\mathbf{y} =& \mathbf{W}_C\mathbf{A}\mathbf{u} + \mathbf{W}_C\mathbf{e} = \\ =& \mathbf{A}_{w_C}\mathbf{u}_{w_C} + \mathbf{e}_{w_C} \end{aligned} \tag{18}$$

where $\mathbf{e}_{w_C} = \mathbf{W}_C\mathbf{e}$ is the whitened measurement error vector.

However, this particular whitening matrix does not allow solving also the second problem. In fact, even assuming uniform distributions for the errors of both magnitudes and phase angles in $\overline{\mathbf{y}}$, the entries of the whitened error vector $\mathbf{e}_{w_C}$ are no longer uniform.

The principal cause of this difference is the polar-to-rectangular transformation applied to the error vector:

$$\mathbf{e} \simeq \mathbf{J}\mathbf{e}_{\rho,\phi} \tag{19}$$

where $\mathbf{e}_{\boldsymbol{\rho},\boldsymbol{\phi}} = [e_{\rho_1},\ldots,e_{\rho_M},e_{\phi_1},\ldots,e_{\phi_M}]^T$. In fact, it is possible to observe that the information on the distributions of $\mathbf{e}_{\boldsymbol{\rho},\boldsymbol{\phi}}$ entries is lost when applying the Jacobian transformation. Moreover, the further application of the whitening matrix $\mathbf{W}_C$ is not able to recover the original distributions.

To prove this, let consider two harmonic phasor measurements (V_1 and $I_{9,10}$, with reference to the test scenario that will be presented in Section IV-A), whose errors on both magnitude and phase angle in $\mathbf{e}_{\boldsymbol{\rho},\boldsymbol{\phi}} = [e_{\rho_{V_1}}, e_{\rho_{I_{9,10}}}, e_{\phi_{V_1}}, e_{\phi_{I_{9,10}}}]^T$ are uniformly distributed. Their possible values have been obtained for 10^6 Monte Carlo (MC) trials. The entries of $\mathbf{e}_{\boldsymbol{\rho},\boldsymbol{\phi}}$ have been randomly extracted according to uniform distributions, whose limits were defined using the "low-uncertainty level" that will be discussed in Section IV-A. During each trial, the polar-to-rectangular transformation (10) has been applied to the measured values, in order to obtain $\mathbf{e} = [e_{V_1}^r, e_{I_{9,10}}^r, e_{V_1}^x, e_{I_{9,10}}^x]^T$. By looking at the histograms of its entries, shown in Fig. 1, it can be seen that the polar-to-rectangular transformation modifies the distributions of the measurement errors.

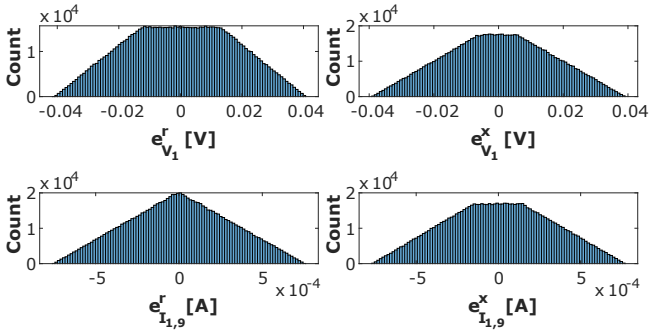

Fig. 1. Histograms of real and imaginary component of voltage and current measurements NOT whitened.

Finally, the error vector has been whitened by means of $\mathbf{W}_C$. In Fig. 2 the entries of the whitened error vector $\mathbf{e}_{w_C} = [e_1^{w_C}, e_2^{w_C}, e_3^{w_C}, e_4^{w_C}]^T$ are shown. It is evident that these distributions are not uniform, as stated previously.

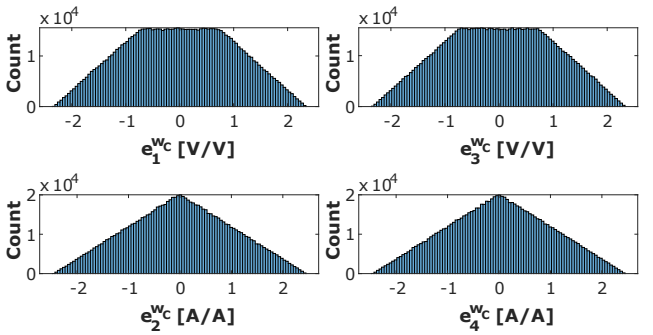

Fig. 2. Histograms of the components of the voltage and current rectangular measurements whitened via $\mathbf{W}_C$.

To overcome this problem, and in order to be able to determine a feasible bound of the error measurement vector, an appropriate whitening matrix is proposed in the following.

B. Proposed whitening matrix

A suitable whitening can recover the information on the initial measurement error distributions, which are modified due to the polar-to-rectangular transformation. The proposed matrix will be labelled as $\mathbf{W}_R$, where the subscript R indicates that this transformation has the feature to recover the information.

Starting from equation (17), among all the infinite solutions that could fit the requirements, the use of the following whitening matrix is proposed:

$$\mathbf{W}_R = \mathbf{\Sigma}_{\boldsymbol{\rho},\boldsymbol{\Phi}}^{-\frac{1}{2}} \mathbf{J}^{-1} \tag{20}$$

The new whitened error vector $\mathbf{e}_{w_R}$ becomes:

$$\mathbf{e}_{w_R} = \mathbf{W}_R \mathbf{e} = \mathbf{\Sigma}_{\boldsymbol{\rho},\boldsymbol{\Phi}}^{-\frac{1}{2}} \mathbf{J}^{-1} \mathbf{e} \tag{21}$$

and it can be directly related to the original error vector, in polar coordinates as follows:

$$\mathbf{e}_{w_R} \simeq \mathbf{\Sigma}_{\boldsymbol{\rho},\boldsymbol{\Phi}}^{-\frac{1}{2}} \mathbf{J}^{-1} \mathbf{J} \mathbf{e}_{\boldsymbol{\rho},\boldsymbol{\Phi}} = \mathbf{\Sigma}_{\boldsymbol{\rho},\boldsymbol{\Phi}}^{-\frac{1}{2}} \mathbf{e}_{\boldsymbol{\rho},\boldsymbol{\Phi}} \tag{22}$$

Observing (15), it is immediate to notice that, in (22), $\mathbf{\Sigma}_{\boldsymbol{\rho},\boldsymbol{\Phi}}^{-\frac{1}{2}}$ has the only effect of re-scaling each component of the magnitude and phase error vector $\mathbf{e}_{\boldsymbol{\rho},\boldsymbol{\Phi}}$ by its standard deviation (measurement standard uncertainty). It is thus possible to affirm that, under the first order approximation due to the linearization of the error propagation and through the whitening matrix $\mathbf{W}_R$, it is possible to obtain a white error that maintains the useful information on the original measurement error distributions that was lost in the polar-to-rectangular transformation.

Consequently, starting from the same harmonic phasor measurements previously considered, the distributions of the whitened error, $\mathbf{e}_{w_R} = [e_1^{w_R}, e_2^{w_R}, e_3^{w_R}, e_4^{w_R}]^T$, obtained by means of the proposed $\mathbf{W}_R$ are shown in Fig. 3.

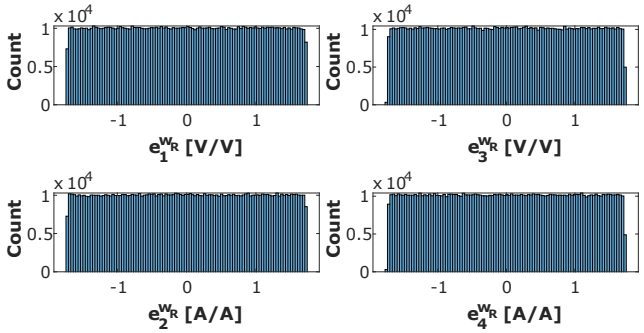

Fig. 3. Histograms of the components of the voltage and current rectangular measurements whitened via $\mathbf{W}_R$.

Thus, starting from magnitude and phase measurement errors uniformly distributed, it is possible to obtain whitened measurement error vectors whose entries are still uniformly distributed. Similar considerations hold for any initial distribution. It is then possible to overcome both problems presented at the beginning of this section.

Moreover, by observing (17) it is possible to notice that all whitened vectors that can be obtained applying any whitening transformation to the same original error vector, have the same energy error. Indeed:

$$\begin{aligned} &\forall \mathbf{Q}: \quad \mathbf{Q}\mathbf{Q}^T = \mathbf{Q}^T\mathbf{Q} = \mathbf{I} \\ &\|\mathbf{W}\mathbf{e}\|_2^2 = \left\| \mathbf{Q}\mathbf{\Sigma}_{\boldsymbol{\rho},\boldsymbol{\Phi}}^{-\frac{1}{2}} \mathbf{J}^{-1}\mathbf{e} \right\|_2^2 = \|\mathbf{Q}\|_2^2 \left\| \mathbf{\Sigma}_{\boldsymbol{\rho},\boldsymbol{\Phi}}^{-\frac{1}{2}} \mathbf{J}^{-1}\mathbf{e} \right\|_2^2 = \\ &\qquad = \left\| \mathbf{\Sigma}_{\boldsymbol{\rho},\boldsymbol{\Phi}}^{-\frac{1}{2}} \mathbf{J}^{-1}\mathbf{e} \right\|_2^2 = \|\mathbf{W}_R\mathbf{e}\|_2^2 \\ &\qquad \Longrightarrow \|\mathbf{e}_w\|_2^2 = \|\mathbf{e}_{w_R}\|_2^2 \end{aligned} \tag{23}$$

where $\mathbf{e}_w \triangleq \mathbf{W}\mathbf{e}$ is the generic whitened error vector. Therefore, if, due to a specific whitening transformation, it is possible to estimate the error energy distribution of the resulting whitened error vector, this estimation holds for all the whitened error vectors that can be obtained from the same error vector.

It is worth noting that computing $\mathbf{W}_R$ is immediate because it is available directly by the construction of $\Sigma_{\mathbf{y}}$.

C. Evaluation of the error energy bound

Once the distributions of the entries of the measurement error vector are known, it is possible to determine the error bound. As shown in Section II-B, this parameter plays a key role in the application of the $(P2)$ problem, and if it is incorrectly evaluated it could lead to a decrease in the performance of the algorithm.

Let consider M harmonic phasor measurements, whose errors, on both magnitude and phase angle, are uniformly distributed. The i-th component of the corresponding $\mathbf{e}_{w_R}$ is a uniform random variable with unitary standard deviation and, by indicating it with $e_{w_R,i}$, it is possible to write:

$$e_{w_R,i} \sim \mathcal{U}(-\sqrt{3}, \sqrt{3}) \;\; \forall i = 1, \ldots, 2M \tag{24}$$

Thus, the energy of the whitened error vector is the sum of squared uniform random variables:

$$\xi_{\mathbf{e}_w} \triangleq \|\mathbf{e}_w\|_2^2 = \|\mathbf{e}_{w_R}\|_2^2 = \sum_{i=1}^{2M} e_{w_R,i}^2 \tag{25}$$

The sum of n squared uniform random variables $\sim \mathcal{U}(-\Delta, \Delta)$ has mean value $\frac{n\Delta^2}{3}$ and standard deviation $\frac{\Delta^2 2\sqrt{n}}{3\sqrt{5}}$. In the case at hand, according to (24), $\Delta = \sqrt{3}$ and $n = 2M$, which leads to:

$$\begin{aligned} \mu_{\xi_{\mathbf{e}_w}} &= \text{mean}(\xi_{\mathbf{e}_w}) \simeq 2M \\ \sigma_{\xi_{\mathbf{e}_w}} &= \text{std}(\xi_{\mathbf{e}_w}) \simeq 2\sqrt{\frac{2}{5}M} \end{aligned} \tag{26}$$

Considering (7), along with the above mentioned inequalities and results in [24], it is possible to set the error bound according to:

$$\epsilon_w^2 = \mu_{\xi_{\mathbf{e}_w}} + \lambda\, \sigma_{\xi_{\mathbf{e}_w}} \tag{27}$$

choosing λ according to the desired confidence level.

In order to verify the validity of (27), starting from a set of 11 harmonic phasor measurements, with the same characteristics of those considered in Section IV-A, the distribution of the error energy has been evaluated. Moreover,

to show graphically that all the whitened error vectors are characterized by the same energy, the histograms of the energy of the whitened errors $\mathbf{e}_{w_C}$ and $\mathbf{e}_{w_R}$ obtained with the two transformations presented above ($\mathbf{W}_C$ and $\mathbf{W}_R$) and evaluated by means of 10^6 MC trials, are reported in Fig. 4. The 95-th and the 99-th percentile of each whitened error energy distribution are represented, respectively, with red and magenta dashed lines, while the value of ϵ_w^2 (estimated by choosing $\lambda = 2$) is denoted with the black dashed line. As expected, it is possible to observe that the two distributions are perfectly identical, with 95-th percentile equal to 29.0630 and the 99-th percentile equals to 32.0938. Moreover, the ϵ_w^2 calculated by means of (27) stays between the 95-th and the 99-th percentile of the whitened error energy distribution (and is equal to 30.3905). Thus, $\lambda = 2$ appears a good compromise in practice to avoid underestimation of $\xi_{\mathbf{e}_w}$ or overestimation of the misfit. Consequently, in the following, $\lambda = 2$ is chosen for the evaluation of the error bound ϵ used in the $(P2)$ formulation.

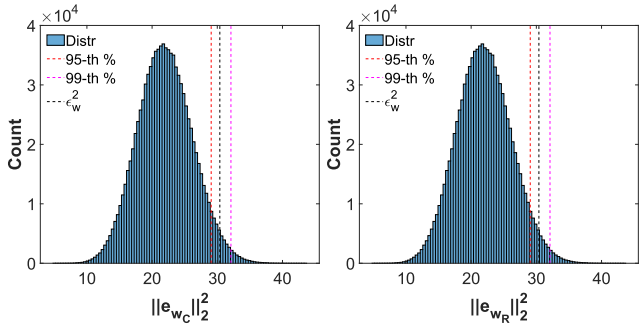

Fig. 4. Histograms of $\xi_{\mathbf{e}_w} = \|\mathbf{e}_{w_C}\|_2^2$ and $\xi_{\mathbf{e}_w} = \|\mathbf{e}_{w_R}\|_2^2$, in the presence of measurements whitened with $\mathbf{W}_C$ and $\mathbf{W}_R$.

IV. HSoE Tests and Results

In order to compare the different performance of the two formulations of the ℓ_1-minimization problem, $(P1)$ and $(P2)$, both algorithms have been implemented in the HSoE framework applied on simulated test distribution grids.

A. Test set-up

The first considered test grid is a small distribution network, shown in Fig. 5, at rated frequency of 60 Hz and nominal voltage $V_n = 4.16$ kV. The system is composed of 13 nodes with a possible polluting load connected to each one of them, with the only exception of node 1, where the substation is connected.

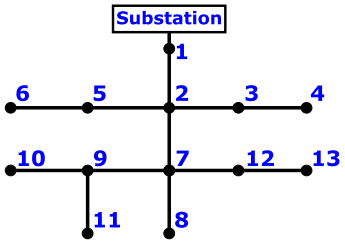

Fig. 5. Scheme of the 13-bus test grid.

Loads are modelled through an ohmic-inductive impedance, whose parameters are defined according to the nominal powers reported in Table I, connected in parallel with an ideal current source that represents the non-linearity of the load, and thus the harmonic pollution injected into the system.

TABLE I
Nominal Loads Configuration

Load	P_n [kW]	Q_n [kvar]
L2	160	110
L3	120	90
L4	170	125
L5	380	220
L6	120	90
L7	70	60
L8	290	210
L9	230	130
L10	490	190
L11	130	90
L12	380	220
L13	170	150

The current injected by the l-th load is obtained by summing up the harmonic contributions of all the considered harmonic orders. In this study, the odd harmonic orders from the 3-rd to the 15-th have been considered, and the magnitude of the pollution level has been defined in percentage with respect to the nominal currents of each load. The default values for each harmonic order are reported in Table II.

TABLE II
Harmonic Forcing Currents Configuration

Harmonic order h	3	5	7	9	11	13	15
Magnitude [%]	5	5	3	3	3	1	1

During the tests, by considering two possible sources simultaneously polluting (thus a sparsity level $S = 2$), all the $N_c = \binom{12}{2} = 66$ couples of polluting loads have been considered. When polluting, the loads have all the harmonics in Table II. To focus on the performance of the proposed solutions and the impact of the uncertainty sources, the nominal loads have been considered in all the tests.

With reference to the analysis of a possible SG scenario, it has been considered that synchronized harmonic phasor measurements, node voltages (V_i, with reference to the i-th node) and branch currents ($I_{i,j}$, with reference to the branch delimited by nodes i and j), derived from PMU-like devices are available in 6 nodes of the network: node 1 (V_1), node 3 (V_3 and $I_{3,4}$), node 5 (V_5 and $I_{5,6}$), node 8 (V_8), node 9 (V_9, $I_{9,10}$ and $I_{9,11}$) and node 12 (V_{12} and $I_{12,13}$). Further analyses on optimal placement of the measurement devices are out of scope of this paper, and thus are not considered in the following.

To assess the validity of the proposed methodologies, as a starting test, both $(P1)$ and $(P2)$ algorithms have been tested in an ideal measurement scenario, neglecting measurement errors. It is evident that these tests do not correspond to the real operating condition of the system, but they are fundamental to establish the best possible performance of the algorithms in this context. In the presence of the ideal conditions for the considered measurement configuration, it was possible

to detect perfectly both polluting loads in each of the N_c considered combinations.

Nevertheless, as presented above and discussed, for example, in [13], measurement uncertainties play instead a key role in HSoE, and their impact on the performance of the estimation algorithms has to be suitably investigated. In the following, the impact of measurement uncertainties on the two different formulations $(P1)$ and $(P2)$ is evaluated by means of MC trials. During each trial, for both magnitude and phase angle of every measured harmonic phasor, the additive term representing the measurement error has been extracted from uniform distributions, whose limits have been defined in accordance with three different uncertainty levels (low, medium, high) summarized in Table III, where the error on the magnitude is referred to the percentage of the measured value.

TABLE III
MAXIMUM MEASUREMENT ERRORS

	Max Magnitude Error [%]	*Max Phase Angle Error* [crad]
low	0.5	0.6
medium	2.5	3
high	5	6

All the simulations have been performed in MATLAB environment, by considering the routines `l1eq_pd` and `l1qc_logbarrier`, for solving the $(P1)$ and the $(P2)$ problems, respectively, which are part of the ℓ_1-MAGIC library presented in [30]. The vectors recovered with the ℓ_1-minimization algorithms are not exactly sparse, as each entry is in general different from zero. Once the solution of the (P1) and (P2) problems is obtained, the S sources with the maximum absolute values are classified as polluters. The ϵ value in (5) has been evaluated by means of the error energy evaluation framework presented in Section III with $\lambda = 2$.

B. Test results

In this section, the performance of the two algorithms is presented and compared. The identification results will be represented by means of the so-called *Recall*, also known as sensitivity, often used in pattern recognition applications and that in our case corresponds to the correct detection rate. Given NS polluting sources and denoting, respectively, with NT and NF the number of true and failed identifications of the polluting sources provided by the algorithm, the recall can be defined as:

$$Recall = \frac{NT}{NT + NF} = \frac{NT}{NS} \tag{28}$$

It is immediate to see that $Recall \in [0, 1]$, where 1 holds when perfect detection is obtained.[1] In this study, the case of two sources polluting simultaneously is assumed and, as mentioned above, 66 different non-repetitive combinations are possible. For each combination of polluting sources, denoted by the subscript $c = \{1, \cdots, N_c\}$, and given $N_{MC} = 1000$ MC trials, it is possible to define the corresponding average $Recall$ as:

$$Recall_c \triangleq \frac{1}{N_{MC}} \sum_{t=1}^{N_{MC}} \frac{NT_{c,t}}{NS_{c,t}} = \frac{\sum_{t=1}^{N_{MC}} NT_{c,t}}{N_{MC} NS} \tag{29}$$

considering that NS is constant for each trial.

Once (29) is defined, it is also possible to consider the overall mean and standard deviation of $Recall_c$ as performance indices of the algorithms:

$$\begin{aligned} \mu_{R_c} &= \frac{\sum_{c=1}^{N_C} Recall_c}{N_C} \\ \sigma_{R_c} &= \sqrt{\frac{\sum_{c=1}^{N_C} (Recall_c - \mu_{R_c})^2}{N_C - 1}} \end{aligned} \tag{30}$$

In Fig. 6, the intervals of $Recall_c$ values together with the mean values are visible for both algorithms and for each uncertainty level, with reference to the 3-rd, 5-th and 7-th harmonic orders. It is possible to observe that, due to the fact that $Recall_c$ has limited range $[0, 1]$, its means are close to the maximum values when uncertainty is low, and the trends are always highly not-symmetric.

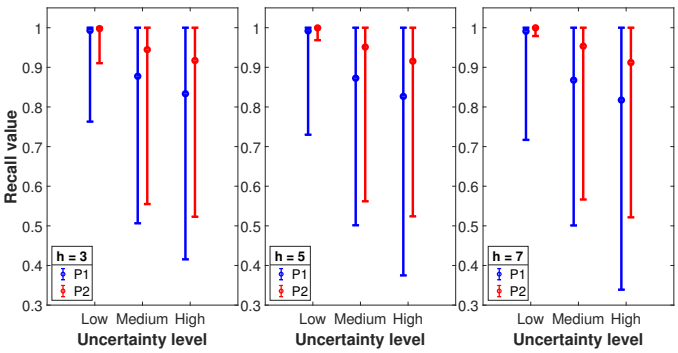

Fig. 6. Recall intervals and mean values, harmonic orders $h = 3$, $h = 5$ and $h = 7$.

In Table IV, the obtained μ_{R_c} and σ_{R_c} for the analysis of the 3-rd, 5-th, and 7-th harmonic orders are reported for $(P1)$ and $(P2)$ by rows, with the different uncertainty levels by columns. As expected, for both algorithms, μ_{R_c} values decrease, while σ_{R_c} increases, when the considered uncertainty level increases. Moreover, it is worth underlying that also the differences between the performance of the two algorithms increase ($(P2)$ has always higher detection performance) with the uncertainty level, which is due to the two different formulations of the problem. In fact, as discussed above, the possibility of including information on the measurement error in the $(P2)$ algorithm, through the definition of the error bound ϵ, is the key to achieve better performance.

It has to be noticed that, while the evaluation of the μ_{R_c} provides information on the overall performance of the two algorithms, the σ_{R_c} value reveals information on the stability

[1] $Recall$ parameter is usually reported together with $Precision$ parameter that in this work is omitted since, in this specific analysis, the parameters assume identical values. Indeed, $Recall$ and $Precision$ parameters express the percentage of correct identifications with respect to the relevant identifications and to the total amount of detection, respectively. In this work, for each trial, the number of polluters and the number of identifications are constant and equal in both cases to $NS = 2$, thus $Recall = Precision$.

TABLE IV
Recall PARAMETERS FOR THE TWO ALGORITHMS (13-BUS TEST CASE)

Harmonic order		Uncertainty level: Low μ_{R_c}	Low σ_{R_c}	Medium μ_{R_c}	Medium σ_{R_c}	High μ_{R_c}	High σ_{R_c}
$h=3$	**(P1)**	0.993	0.032	0.878	0.187	0.833	0.219
	(P2)	0.998	0.013	0.945	0.128	0.917	0.151
$h=5$	**(P1)**	0.992	0.037	0.873	0.194	0.827	0.222
	(P2)	0.999	0.004	0.951	0.112	0.916	0.148
$h=7$	**(P1)**	0.991	0.039	0.868	0.200	0.817	0.223
	(P2)	0.999	0.003	0.953	0.106	0.912	0.148

of the performance across different conditions. In particular, the higher σ_{R_c} values for $(P1)$ suggest that the identification provided by $(P1)$ is less stable towards the variation of polluting sources.

By focusing on the identification results of each polluting source, it is possible to further highlight the different performance results of $(P1)$ and $(P2)$. In this regard, in Fig. 7 the detection of load L2 is reported, with reference to the 5-th harmonic order, in percentage with respect to the 1000 MC trials used for each possible combination of polluting loads. In the x-axis the second polluting load for each scenario is reported, whereas blue and red lines denote, respectively, the average detection rate of load $L2$ provided by $(P1)$ and $(P2)$. By looking at the top plot, which refers to the lower uncertainty level considered in the tests, it is possible to see that both algorithms correctly identify load $L2$ when combined with any other load. On the contrary, by looking at the mid and bottom plots, which refer to the medium and high level of uncertainty respectively, it is evident that the performance of both algorithms decreases, and especially that obtained by $(P1)$ algorithm. When the lowest accuracy is assumed, $(P2)$ algorithm detects correctly load $L2$ more than 55% of the times, for any possible combination of polluting sources, while $(P1)$ detection reaches the same result only for one of the 11 combinations.

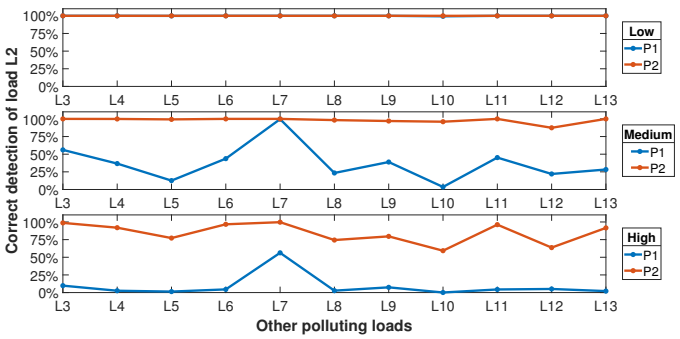

Fig. 7. Detection of load $L2$, harmonic order $h=5$.

In Fig. 8 and in Fig. 9, the percentage of detection of loads $L7$ and $L11$, when polluting with the other loads, is reported. These figures underline how the performance of both $(P1)$ and $(P2)$ can vary significantly. While load $L11$ is always detected, despite the considered uncertainty level, the detection of load $L7$ is more sensitive to the increase in measurement uncertainty. In particular, it is evident how, even when the effects of measurement uncertainties are correctly taken into account, the metrological characteristics of the measurement devices play a key role in the detection of the polluting sources, and high-accuracy instruments could lead to significantly better detection rates.

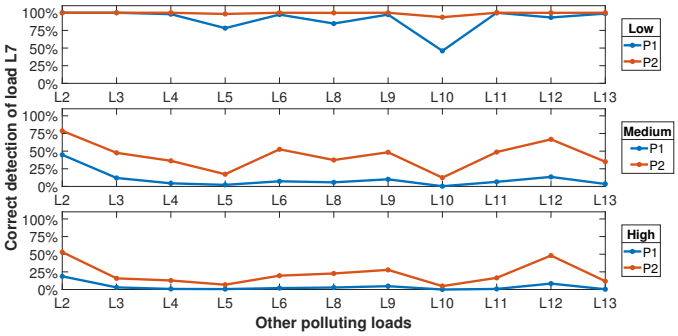

Fig. 8. Detection of load $L7$, harmonic order $h=5$.

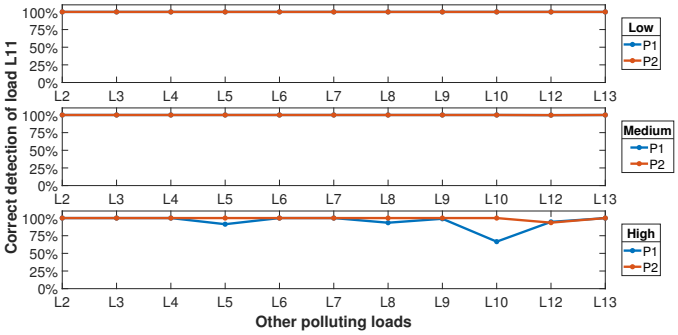

Fig. 9. Detection of load $L11$, harmonic order $h=5$.

C. Tests on a larger network

To further test the validity of the proposed technique, additional analyses have been conducted on a larger distribution network, characterized by 49 nodes and 20 measurement points, whose characteristics are reported in the Appendix. Furthermore, to give a wider perspective, the performance of both $(P1)$ and $(P2)$ algorithms are here compared also with the performance of a weighted least square minimum norm technique (WLS for brevity in the following), already proposed in [13] as a term of comparison.

In Table V, the comparison results are presented following the same test approach as in the previous tests (that is testing all the $N_c = \binom{48}{2} = 1128$ possible polluting couples for three uncertainty levels and 1000 MC trials), with reference to the 3-rd and the 5-th harmonic orders, by means of the mean and standard deviation of the *Recall* indicator, as defined in (30). The results show that the proposed $(P2)$ algorithm, thanks to a correct uncertainty modelling, clearly outperforms the other two methods in all the tested conditions.

V. CONCLUSIONS

The identification of the harmonic sources in distribution networks represents an important task for the system operator,

TABLE V
Recall PARAMETERS FOR THE THREE ALGORITHMS (49-BUS TEST CASE)

Harmonic order		Uncertainty level: Low μ_{R_c}	Low σ_{R_c}	Medium μ_{R_c}	Medium σ_{R_c}	High μ_{R_c}	High σ_{R_c}
$h=3$	**WLS**	0.823	0.259	0.815	0.259	0.743	0.243
	(P1)	0.945	0.114	0.829	0.240	0.743	0.242
	(P2)	0.989	0.058	0.941	0.135	0.893	0.169
$h=5$	**WLS**	0.823	0.258	0.813	0.259	0.733	0.241
	(P1)	0.945	0.119	0.826	0.242	0.731	0.239
	(P2)	0.989	0.055	0.946	0.125	0.894	0.165

that could act directly on the source of the problem, to reduce the negative effects. The use of ad-hoc designed algorithms, such as compressive sensing-based methodologies, allows overcoming the problems related to the limited availability of power quality meters. Nevertheless, the performance of the identification algorithms depends on the measurement uncertainties, and their impact cannot be neglected.

In this paper, starting form the theoretical aspects involved in the evaluation of the measurement uncertainties, and the reduction of their impact on HSoE algorithms, a new formulation of the ℓ_1-minimization problem has been proposed. In order to maximize the performance of the proposed formulation, a whitening matrix allowing the recovery of information on the distributions of the measurement errors, and thus the estimation of the corresponding bounds, has been presented. The effectiveness of the proposed solution has been tested by comparing its detection performance to both a previous formulation of the ℓ_1-minimization and a weighted least square minimum norm approach. The tests have been performed in a controlled environment through simulations performed on two distribution grids, taking into account different scenarios for the possible measurement systems available on the grids. The results underline how the proposed formulation, presenting an appropriate modelling of measurement uncertainties, achieves the best detection performance. This modelling appears then as the necessary step to make the algorithms more robust in view of future on-field implementation by system operators.

APPENDIX

MODEL OF THE 49-BUS TEST SYSTEM

The main characteristics of the 49-bus test system, respectively in terms of topology, nominal loads and measurement configuration, are presented in Fig. 10, Table VI and Table VII.

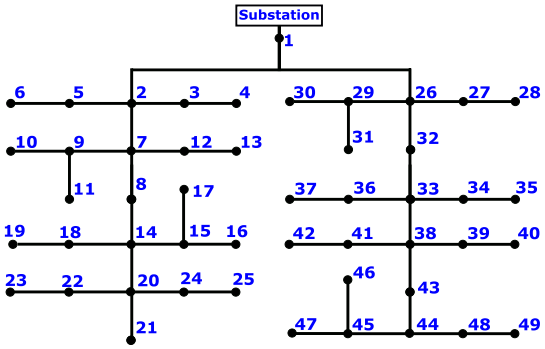

Fig. 10. Topology of the 49-bus test grid.

TABLE VI
NOMINAL LOADS CONFIGURATION OF THE 49-BUS TEST SYSTEM

Loads	P_n [kW]	Q_n [kvar]
L2, L20, L33, L38	48	33
L3, L21, L34, L39	36	27
L4, L22, L35, L40	51	38
L5, L23, L36, L41	81	48
L6, L24, L37, L42	36	27
L7, L14, L26, L44	27	18
L8, L25, L32, L43	42	24
L9, L15, L29, L45	69	39
L10, L16, L30, L46	78	39
L11, L17, L31, L47	39	27
L12, L18, L27, L48	90	45
L13, L19, L28, L49	51	45

TABLE VII
MEASUREMENT CONFIGURATION OF THE 49-BUS TEST SYSTEM

Bus Voltage	V_1, V_3, V_5, V_8, V_9, V_{12}, V_{15}, V_{18}, V_{21}, V_{22} V_{24}, V_{27}, V_{29}, V_{32}, V_{34}, V_{36}, V_{39}, V_{41}, V_{45}, V_{48}
Branch Current	$I_{3,4}$, $I_{5,6}$, $I_{9,10}$, $I_{9,11}$, $I_{12,13}$, $I_{15,16}$ $I_{15,17}$, $I_{18,19}$, $I_{22,23}$, $I_{24,25}$, $I_{27,28}$, $I_{29,30}$ $I_{29,31}$, $I_{34,35}$, $I_{36,37}$, $I_{39,40}$, $I_{41,42}$, $I_{45,46}$, $I_{45,47}$, $I_{48,49}$

REFERENCES

[1] M. H. J. Bollen, "What is power quality?" *Electric Power Systems Research*, vol. 66, no. 1, pp. 5–14, Jul. 2003.

[2] K. K. C. Yu, N. R. Watson, and J. Arrillaga, "Error analysis in static harmonic State estimation: a statistical approach," *IEEE Trans. Power Del.*, vol. 20, no. 2, pp. 1045–1050, Apr. 2005.

[3] C. F. M. Almeida and N. Kagan, "Harmonic state estimation through optimal monitoring systems," *IEEE Trans. Smart Grid*, vol. 4, no. 1, pp. 467–478, Mar. 2013.

[4] C. Rakpenthai, S. Uatrongjit, N. R. Watson, and S. Premrudeep-reechacharn, "On harmonic state estimation of power system with uncertain network parameters," *IEEE Trans. Power Syst.*, vol. 28, no. 4, pp. 4829–4838, Nov. 2013.

[5] Y. Xi *et al.*, "Harmonic estimation in power systems using an optimised adaptive kalman filter based on pso-ga," *IET Generation, Transmission Distribution*, vol. 13, no. 17, pp. 3968–3979, 2019.

[6] J. Mazumdar, R. G. Harley, F. C. Lambert, G. K. Venayagamoorthy, and M. L. Page, "Intelligent tool for determining the true harmonic current contribution of a customer in a power distribution network," *IEEE Trans. Ind. Appl.*, vol. 44, no. 5, pp. 1477–1485, Sep. 2008.

[7] X. Zhu, C. Shen, and X. Ren, "Harmonic detection method using APFFT and neural network," in *2013 5th Int. Conf. Intelligent Human-Machine Syst. and Cybernetics*, Hangzhou, China, Aug. 2013, pp. 356–359.

[8] V. K. Tiwari and S. K. Jain, "Hardware implementation of polyphase-decomposition-based wavelet filters for power system harmonics estimation," *IEEE Trans. Instrum. Meas.*, vol. 65, no. 7, pp. 1585–1595, 2016.

[9] R. Sinvula, K. M. Abo-Al-Ez, and M. T. Kahn, "Harmonic source detection methods: A systematic literature review," *IEEE Access*, vol. 7, pp. 74 283–74 299, 2019.

[10] G. D'Antona, C. Muscas, P. A. Pegoraro, and S. Sulis, "Harmonic source estimation in distribution systems," *IEEE Trans. Instrum. Meas.*, vol. 60, no. 10, pp. 3351–3359, Oct. 2011.

[11] G. D'Antona, C. Muscas, and S. Sulis, "Localization of nonlinear loads in electric systems through harmonic source estimation," *IEEE Trans. Instrum. Meas.*, vol. 60, no. 10, pp. 3423–3430, Oct. 2011.

[12] D. Carta, C. Muscas, P. A. Pegoraro, and S. Sulis, "Harmonics detector in distribution systems based on compressive sensing," in *IEEE Int. Workshop on Appl. Meas. for Power Syst. (AMPS)*, Liverpool, UK, Sep. 2017, pp. 1–5.

[13] D. Carta, C. Muscas, P. A. Pegoraro, and S. Sulis, "Identification and estimation of harmonic sources based on compressive sensing," *IEEE Trans. Instrum. Meas.*, vol. 68, no. 1, pp. 95–104, Jan. 2019.

[14] A. Galli, G. Frigo, D. Chindamo, A. Depari, M. Gadola, and G. Giorgi, "Denoising ECG signal by CSTFM algorithm: Monitoring during motorbike and car races," *IEEE Trans. Instrum. Meas.*, vol. 68, no. 7, pp. 2433–2441, 2019.

[15] J. Zhang, Z. L. Yu, Z. Gu, Y. Li, and Z. Lin, "Multichannel electrocardiogram reconstruction in wireless body sensor networks through weighted $\ell_{1,2}$ minimization," *IEEE Trans. Instrum. Meas.*, vol. 67, no. 9, pp. 2024–2034, 2018.

[16] S. Rousseau and D. Helbert, "Compressive color pattern detection using partial orthogonal circulant sensing matrix," *IEEE Trans. Image Process.*, vol. 29, pp. 670–678, 2020.

[17] E. Balestrieri, L. De Vito, F. Picariello, and I. Tudosa, "A method exploiting compressive sampling for localization of radio frequency emitters," *IEEE Trans. Instrum. Meas.*, vol. 69, no. 5, pp. 2325–2334, 2020.

[18] K. Duda, T. P. Zieliński, A. Bień, and S. H. Barczentewicz, "Harmonic phasor estimation with flat-top fir filter," *IEEE Trans. Instrum. Meas.*, vol. 69, no. 5, pp. 2039–2047, 2020.

[19] G. Frigo, A. Derviškadić, P. A. Pegoraro, C. Muscas, and M. Paolone, "Harmonic phasor measurements in real-world PMU-based acquisitions," in *IEEE Int. Instr. and Meas. Technol. Conf. (I2MTC)*, Auckland, NZ, 2019, pp. 1–6.

[20] G. Crotti, D. Gallo, D. Giordano, C. Landi, M. Luiso, and M. Modarres, "Frequency response of mv voltage transformer under actual waveforms," *IEEE Trans. Instrum. Meas.*, vol. 66, no. 6, pp. 1146–1154, 2017.

[21] M. Faifer, C. Laurano, R. Ottoboni, S. Toscani, and M. Zanoni, "Harmonic distortion compensation in voltage transformers for improved power quality measurements," *IEEE Trans. Instrum. Meas.*, vol. 68, no. 10, pp. 3823–3830, 2019.

[22] A. Cataliotti *et al.*, "Compensation of nonlinearity of voltage and current instrument transformers," *IEEE Trans. Instrum. Meas.*, vol. 68, no. 5, pp. 1322–1332, 2019.

[23] D. Carta, C. Muscas, P. A. Pegoraro, A. V. Solinas, and S. Sulis, "Impact of measurement uncertainties on compressive sensing-based harmonic source estimation algorithms," in *IEEE Int. Instr. and Meas. Technol. Conf. (I2MTC)*, Dubrovnik, Croatia, May 2020.

[24] E. J. Candès, J. K. Romberg, and T. Tao, "Stable signal recovery from incomplete and inaccurate measurements," *Commun. on Pure and Appl. Math.*, vol. 59, no. 8, pp. 1207–1223, 2006.

[25] D. L. Donoho, "For most large underdetermined systems of linear equations the minimal ℓ_1-norm solution is also the sparsest solution," *Commun. on Pure and Appl. Math.*, vol. 59, no. 6, pp. 797–829, 2006.

[26] J. A. Tropp, "Greed is good: algorithmic results for sparse approximation," *IEEE Trans. Inf. Theory*, vol. 50, no. 10, pp. 2231–2242, 2004.

[27] E. J. Candes and T. Tao, "Decoding by linear programming," *IEEE Trans. Inf. Theory*, vol. 51, no. 12, pp. 4203–4215, Dec. 2005.

[28] E. J. Candes, J. Romberg, and T. Tao, "Robust uncertainty principles: exact signal reconstruction from highly incomplete frequency information," *IEEE Trans. Inf. Theory*, vol. 52, no. 2, pp. 489–509, 2006.

[29] JCGM, "Evaluation of data - guide to the expression of uncertainty in measurement," *JCGM 100:2008*, Sep. 2008.

[30] E. Candes and J. Romberg, "l1-magic : Recovery of sparse signals via convex programming," 2005. [Online]. Available: https://statweb.stanford.edu/~candes/software/l1magic/downloads/l1magic.pdf

Daniele Carta (S'18) received the M.S. degree (cum laude) in Electrical Engineering and the Ph.D. degree in Industrial Engineering from the University of Cagliari, Cagliari, Italy, in 2016 and 2020, respectively. He is currently a research fellow in the Electrical and Electronic Measurements Group with the Department of Electrical and Electronic Engineering at same University.

His research activity focuses on: state estimation, fault location, and power quality issues in distribution grids.

Carlo Muscas (M'98, SM'15) received the M.S. degree (cum laude) in electrical engineering from the University of Cagliari, Cagliari, Italy, in 1994. He was an Assistant Professor and an Associate Professor with the University of Cagliari from 1996 to 2001 and from 2001 to 2017, respectively, where he has been a Full Professor of electrical and electronic measurement since 2017. He has authored and coauthored more than 150 scientific articles.

His current research interests include the measurement of synchronized phasors, the implementation of distributed measurement systems for a modern electric grid, and the study of power quality phenomena.

Prof. Muscas is currently the Chairman of the TC 39 Measurements in Power Systems of the IEEE Instrumentation and Measurement Society.

Antonio Vincenzo Solinas received the M.S. degree in Electronic Engineering from University of Cagliari, Italy, in 2000. Since then, he worked as an R&D manager on audio and video acquisition, compression and transmission over IP.

He is currently a Ph.D. student in the Electrical and Electronic Measurements Group with the Department of Electrical and Electronic Engineering at the University of Cagliari.

Paolo Attilio Pegoraro (M'06-SM'19) received the M.S. (cum laude) degree in telecommunications engineering and the Ph.D. degree in electronic and telecommunications engineering from the University of Padova, Padua, Italy, in 2001 and 2005, respectively.

From 2015 to 2018 he was an Assistant Professor with the Department of Electrical and Electronic Engineering, University of Cagliari, Cagliari, Italy, where he is currently Associate Professor. He has authored or co-authored over 110 scientific papers. His current research interests include the development of new measurement techniques for modern power networks.

Dr. Pegoraro is a member of IEEE Instrumentation and Measurement Society TC 39 (Measurements in Power Systems) and of IEC TC 38/WG 47. He is an Associate Editor of the IEEE Transactions on Instrumentation and Measurement.

Sara Sulis (M'06-SM'19) received the M.S. degree in electrical engineering and the Ph.D. degree in industrial engineering from the University of Cagliari, Cagliari, Italy, in 2002 and 2006, respectively.

She is currently an Associate Professor of electrical and electronic measurements with the University of Cagliari. Dr. Sulis is a member of the IEEE Instrumentation and Measurement Society, of the IEEE TC 39 "Measurements in Power Systems", and of the CENELEC TC 38 "Instrument Transformers". She has authored or co-authored more than 100 scientific papers. Her current research interests include distributed measurement systems designed to perform state estimation and harmonic sources estimation of distribution networks.